Annals of Nuclear Energy 51 (2013) 167–180

Contents lists available at SciVerse ScienceDirect

Annals of Nuclear Energy

journal homepage: www.elsevier.com/locate/anucene

A numerical study of flow and mixing characteristics inside the chimney structure of a pool type research reactor

Samiran Sengupta [a,*], P.K. Vijayan [b], K. Sasidharan [a], V.K. Raina [c]

[a] Research Reactor Design & Projects Division, Bhabha Atomic Research Centre, Mumbai 400 085, India
[b] Reactor Engineering Division, Bhabha Atomic Research Centre, Mumbai 400 085, India
[c] Reactor Group, Bhabha Atomic Research Centre, Mumbai 400 085, India

ARTICLE INFO

Article history:
Received 18 January 2012
Received in revised form 13 August 2012
Accepted 15 August 2012
Available online 9 October 2012

Keywords:
Chimney structure
k–ε Turbulence model
Mixing
Stagnation depth

ABSTRACT

Numerical studies were performed to examine the effects of flow velocities of opposing streams on the flow pattern and turbulent mixing characteristics in a three-dimensional chimney structure using CFD code PHOENICS. This chimney structure facilitates guiding of the radioactive water from the reactor core (i.e., core flow) towards the side outlet nozzles and simultaneously drawing out water from the reactor pool through the chimney top. The radioactive water flows upward and has a tendency to reach to the pool top through the chimney top which is open for fuel and isotope handling. The chimney design allows drawing out a part of the pool water in the downward direction to suppress the upward flowing radioactive water jet. This downward flow through the chimney is compensated by providing additional core bypass flow to the pool. Analyses were carried out on 1:1 chimney structure and also on 1/6th scaled down chimney model to understand the similarity of behaviour of the model and the prototype. Mass flow rate of upward flowing water (i.e. core flow) is considered to be 750 kg/s and core bypass flow is varied from 0% to 15% that of the core flow. In the model study, mass flow rate was varied from 8.33 to 25 kg/s and core bypass flow was considered to vary from 0% to 15%. Flow mixing pattern inside the chimney and the non-dimensional stagnation depth was predicted for the model and the prototype. It was observed that there is a good similarity in behaviour of the prototype and model.

1. Introduction

Pool type research reactor often gets preference for isotope production and carrying out various irradiation experiments, due to its simpler design with easy accessibility from the core top. But due to its open top, when core is cooled through forced upward flow, core outlet radioactive water has a tendency to reach towards the pool top due to inertia and buoyancy leading to increase in radiation level at the pool top. Due to limitation of the pool height from the consideration of clear visibility of the core from the pool top (to facilitate fuel and isotope handling operation), upward flow through the core becomes the only choice for this type of reactor to create larger driving pressure differential for providing larger flow velocity of coolant through the core with higher reactor power density. Since, pool top activity level should be limited during normal operation; these reactors often use an open chimney structure at the reactor core outlet in order to prevent radioactive coolant reaching the pool top. A typical example is High Flux Research Reactor (HFRR) being developed at BARC (Chafle et al., 2009).

A simplified flow diagram of the primary coolant system of the HFRR is given in Fig. 1. The reactor core cooling takes place by sending upward flow through the HFRR core (Sengupta et al., 2010a). The radioactive hot water from the core outlet is guided through the chimney and is drawn by a set of pumps through the two side outlet nozzles of the chimney. The radioactive hot water is then passed through delay tanks to decay down the activity level mainly caused by N^{16} radio-nuclides and subsequently it is sent through the heat exchangers where heat is transferred to the secondary coolant. Cold primary coolant water from heat exchanger outlet is sent back to the inlet plenum at the bottom of the reactor core inside the pool. A part of cold water is also sent to the pool which bypasses the core and is drawn through the opening of the chimney top by the operating pumps. This flow is commonly named as core bypass. Flow mixing of core flow and the core bypass inside the chimney is explained in the following section.

2. Turbulent flow mixing inside chimney structure

A schematic flow diagram of flow mixing inside the chimney structure is shown in Fig. 2. The bottom of the chimney sees a strong upward flow from the core outlet (A), while at the open top of the chimney (B) a downward flow only is allowed (to limit

* Corresponding author. Address: Research Reactor Design & Projects Division, Dhruva Complex, Bhabha Atomic Research Centre, Mumbai 400 085, India. Tel.: +91 22 25595610; fax: +91 22 25505311.
E-mail address: samiran_sengupta@yahoo.co.in (S. Sengupta).

0306-4549/$ - see front matter © 2012 Elsevier Ltd. All rights reserved.
http://dx.doi.org/10.1016/j.anucene.2012.08.008

Nomenclature

D	diameter of chimney (m)
g	acceleration due to gravity (m/s^2)
k	turbulent kinetic energy (J)
L	length scale of chimney (m)
Red	Reynolds number, $\frac{\rho U_m D_m}{\mu}$
Red*	Reynolds number, $\frac{\rho U_b D_b}{\mu}$
S	stagnation depth (m)
S^*	non-dimensional stagnation depth
T	temperature (K)
U	mean fluid velocity (m/s)
W	mass flow (kg/s)

Symbols

ρ	fluid density (kg/m^3)
β	volumetric expansion coefficient (K^{-1})
ε	turbulence energy dissipation rate (W)
μ	viscosity (N s/m^2)
υ	kinematic viscosity (m^2/s)

Subscripts

b	branch/bypass flow
in	inlet
m	main flow
p	bulk fluid in pool

pool top radioactivity level). Both upward flow from the bottom and downward flow from the top mixes together just before the side nozzles of the chimney and is sucked out of the chimney with the help of pumps through outlet lines (C1, C2) of two loops of the primary coolant pump. The downward flow into the chimney from the pool is compensated by providing core bypass flow from each loop (D1, D2) into the pool. Turbulent mixing behaviour inside this chimney being complex, a 1/6th scaled down model (Sengupta et. al., 2010b) has been designed. The computational studies are carried out for the scaled down model as well as the prototype and the stagnation depth (i.e., the depth where the upward flow velocity of the core outlet water becomes zero with respect to the top opening edge of the chimney) is predicted for various flow cases. The objective of these simulations is to study the effect of core flow, core bypass flow on the stagnation depth for the prototype as well as model and to understand the relative importance of inertia force, viscous force and buoyancy force. The details of the prototype and the scaled down model considered in the CFD simulation are shown in Table 1.

3. Dimensionless numbers

The dimensionless numbers describing the turbulent mixed convection inside the chimney are defined considering the relevant parameters shown in Fig. 2. The total core bypass flow is W_b, which is distributed through two inlets into the pool. The core outlet flow velocity is U_{in} and fluid temperature is T_{in}. Pool water temperature is T_p. The core bypass flow inlet temperature is also T_p. Height of the chimney where in flow mixing takes place is L.

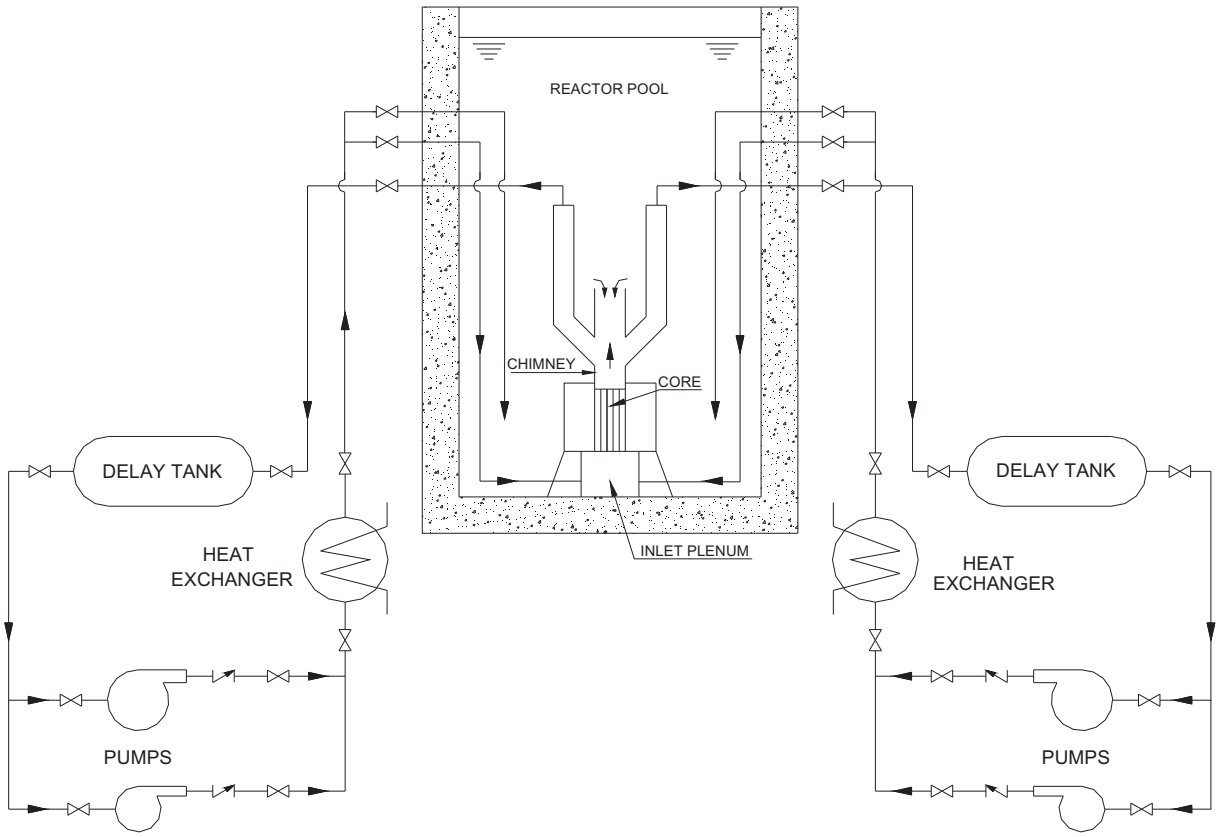

Fig. 1. Simplified flow diagram of primary coolant system of HFRR.

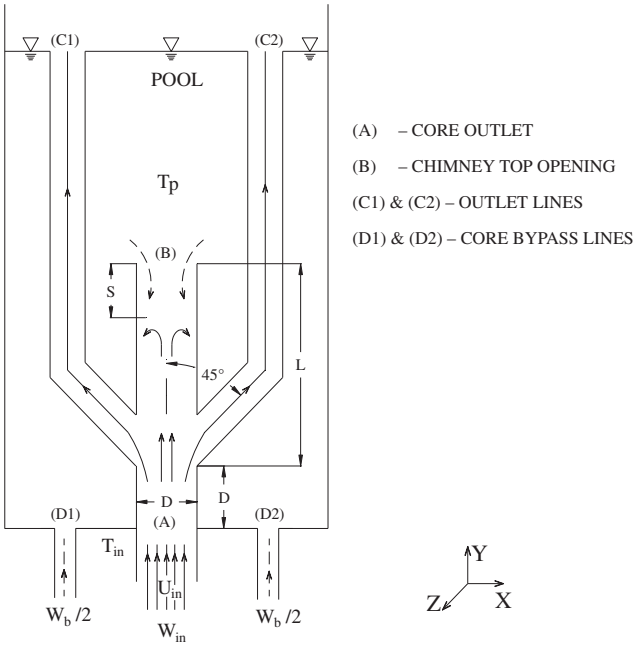

Fig. 2. Schematic diagram of mixing of flow streams inside the chimney structure.

Table 1
Details of prototype and scaled down model.

Parameter	Prototype	Model
Fluid	Light water	Light water
Chimney diameter	600 mm	100 mm
Chimney height	3600 mm	600 mm
Side outlet nozzle area		
(i) Slit height	(i) 300 mm	(i)50 mm
(ii) Slit width	(ii) 600 mm	(ii)100 mm
Side outlet nozzle inclination angle	45°	45°
Fluid temperature		
Chimney top entry	40 °C	40 °C
Chimney bottom entry	49 °C	49 °C

$$\text{Reynolds number, Re} = \frac{\rho U_{in} L}{\mu} \tag{1}$$

$$\text{Grashof number, Gr} = \frac{g\beta(T_{in} - T_p)L^3}{\upsilon^2} \tag{2}$$

$$\text{Richardson number, Ri} = \frac{g\beta(T_{in} - T_p)L}{U_{in}^2} \tag{3}$$

The Reynolds number (Re) shows the significance of the inertia force to viscous force. Grashof (Gr) number shows the affect of buoyancy force to that of the viscous force. Richardson number (Ri) shows the importance of natural convection relative to the forced convection. In addition, two more dimensionless numbers (Re^* and Ri^*) is considered to take into account the ratio between core flow and bypass flow as defined below. Re^* signifies the affect downward inertia force in suppressing the upward flow jet. Ri^* signifies the more pronouncing effect of buoyancy force against the downward forced flow. These numbers are defined as follows:

$$Re^* = \frac{\rho U_{in} L}{\mu}\left(\frac{W_b}{W_{in}}\right) \tag{4}$$

$$Ri^* = \frac{g\beta(T_{in} - T_\alpha)L}{U_{in}^2}\left(\frac{W_{in}}{W_b}\right)^2 \tag{5}$$

4. Computational data matrix

In the present study various parameters considered for the analysis for the scaled down model is shown in Table 2a. Their corresponding non-dimensional numbers are also indicated in the table. Twenty simulations are carried out considering core outlet temperature (T_{in}) as 49 °C and pool temperature (T_p) as 40 °C for the model. In addition, 20 more analyses were carried out with T_{in} and T_p as equal (both 40 °C) to eliminate the buoyancy force due to temperature difference. The difference in results is attributed as caused due to buoyancy. The range of parameters considered in the scaled down model is based on the philosophy of scaling and preservation of non-dimensional numbers to the extent of feasibility (Sengupta et al., 2010b). Range of Reynolds number (Re) considered in the simulation is 1×10^6–3×10^6. Grashof number (Gr) is 1.55×10^{10} based on characteristic dimension of chimney height (L). Richardson number (Ri) range is from 0.002 to 0.017.

Parameters for the prototype and their non-dimensional number are indicated in Table 2b. Reynolds number (Re) for the prototype is 1.44×10^7. Grashof number (Gr) and Richardson number (Ri) are 3.34×10^{12} and 0.016 respectively.

In order to compare the results of the model and the prototype, stagnation depth (S) is non-dimensionalised with respect to the chimney height (L) to obtain non-dimensional stagnation depth (S^*) using the following relation:

$$S^* = \frac{S}{L} \tag{6}$$

Table 2a
Computational data matrix (Model).

Sr. no.	Core flow (kg/s)	Bypass flow (%)	Re	Gr	Ri	Re^*	Ri^*
1	25	0	2.87×10^6	1.55×10^{10}	0.0019	–	–
2	25	5	2.87×10^6	1.55×10^{10}	0.0019	1.44×10^5	0.749
3	25	10	2.87×10^6	1.55×10^{10}	0.0019	2.87×10^5	0.187
4	25	15	2.87×10^6	1.55×10^{10}	0.0019	4.31×10^5	0.083
5	20.83	0	2.39×10^6	1.55×10^{10}	0.0027	–	–
6	20.83	5	2.39×10^6	1.55×10^{10}	0.0027	1.20×10^5	1.079
7	20.83	10	2.39×10^6	1.55×10^{10}	0.0027	2.39×10^5	0.270
8	20.83	15	2.39×10^6	1.55×10^{10}	0.0027	3.59×10^5	0.120
9	16.67	0	1.92×10^6	1.55×10^{10}	0.0042	–	–
10	16.67	5	1.92×10^6	1.55×10^{10}	0.0042	9.58×10^4	1.686
11	16.67	10	1.92×10^6	1.55×10^{10}	0.0042	1.92×10^5	0.422
12	16.67	15	1.92×10^6	1.55×10^{10}	0.0042	2.87×10^5	0.187
13	12.5	0	1.44×10^6	1.55×10^{10}	0.0075	–	–
14	12.5	5	1.44×10^6	1.55×10^{10}	0.0075	7.18×10^4	2.998
15	12.5	10	1.44×10^6	1.55×10^{10}	0.0075	1.44×10^5	0.749
16	12.5	15	1.44×10^6	1.55×10^{10}	0.0075	2.15×10^5	0.333
17	8.33	0	9.58×10^5	1.55×10^{10}	0.0169	–	–
18	8.33	5	9.58×10^5	1.55×10^{10}	0.0169	4.79×10^4	6.745
19	8.33	10	9.58×10^5	1.55×10^{10}	0.0169	9.58×10^4	1.686
20	8.33	15	9.58×10^5	1.55×10^{10}	0.0169	1.43×10^5	0.749

Table 2b
Computational data matrix (Prototype).

Sr. no.	Core flow (kg/s)	Bypass flow (%)	Re	Gr	Ri	Re^*	Ri^*
1	750	0	1.44×10^7	3.34×10^{12}	0.016	–	–
2	750	5	1.44×10^7	3.34×10^{12}	0.016	7.18×10^5	6.475
3	750	10	1.44×10^7	3.34×10^{12}	0.016	1.44×10^6	1.619
4	750	15	1.44×10^7	3.34×10^{12}	0.016	2.15×10^6	0.719

Stagnation depth (S) is defined as the depth from the top opening edge of the chimney to the position where the upward flow velocity of the core outlet water becomes zero (at the central axis of the chimney).

5. Computational methodology

In the present work, three dimensional simulation of chimney along with reactor pool is done. Computational fluid dynamics software PHOENICS version 3.6 (Ludwig, 2004) is used for carrying out all the simulations. The continuity, momentum and energy equations in Cartesian co-ordinates are solved in this computer code. The solution domain is subdivided into a number of control volumes, each associated with a grid point, where the scalar variables such as pressure, temperature, and concentration are stored. The control volumes for the velocity are staggered in relation to the control volumes for the scalar variables. The buoyancy force is accounted by using Boussinesq model. This model assumes that the density is constant but modifies the source term of the momentum equation to account for the buoyancy effect. Since the governing equations are non-linear and coupled, these are solved by SIMPLE algorithm (Patankar, 1980). The implicit equations are solved by TDMA. For turbulence modelling, Reynolds averaged form of the continuity, momentum and energy equations are solved using standard k–ε turbulence model. The values of the constants used in the turbulence model is shown in Table 3.

Table 3
Values of constants in the k–ε model.

c_μ	$c_{1\varepsilon}$	$c_{2\varepsilon}$	σ_k	σ_ε
0.09	1.44	1.92	1.0	1.3

The modelling prepared in PHOENICS for full scale as well as 1/6th scaled down model is shown in Fig. 3. The range of Reynolds number based on pipe diameter for all the simulation cases of model is Red ~ 2–6×10^5 and Red$^* \sim 1$–9×10^4. For the full scale prototype, the range is Red $\sim 3 \times 10^6$ and Red$^* \sim 1.5$–4.5×10^5.

5.1. Computational domain

The computational domain considered for the prototype is 4 m $\times$ 7.5 m $\times$ 1.2 m. Calculation is done with $(190 \times 200 \times 40)$ grid points. The chimney geometry simulated is similar in dimensions as that of the full scale size. The reactor pool dimension is 5 m diameter and about 9 m height from the top of the reactor core. Due to the limitation of the number of grid points, the pool dimension considered in the simulation is 4 m $\times$ 1.2 m $\times$ 7.5 m height. In addition, free surface modelling at the interface between pool water and air at the top is not modelled considering larger pool water depth above the chimney top. The computational domain considered for the scaled down model is

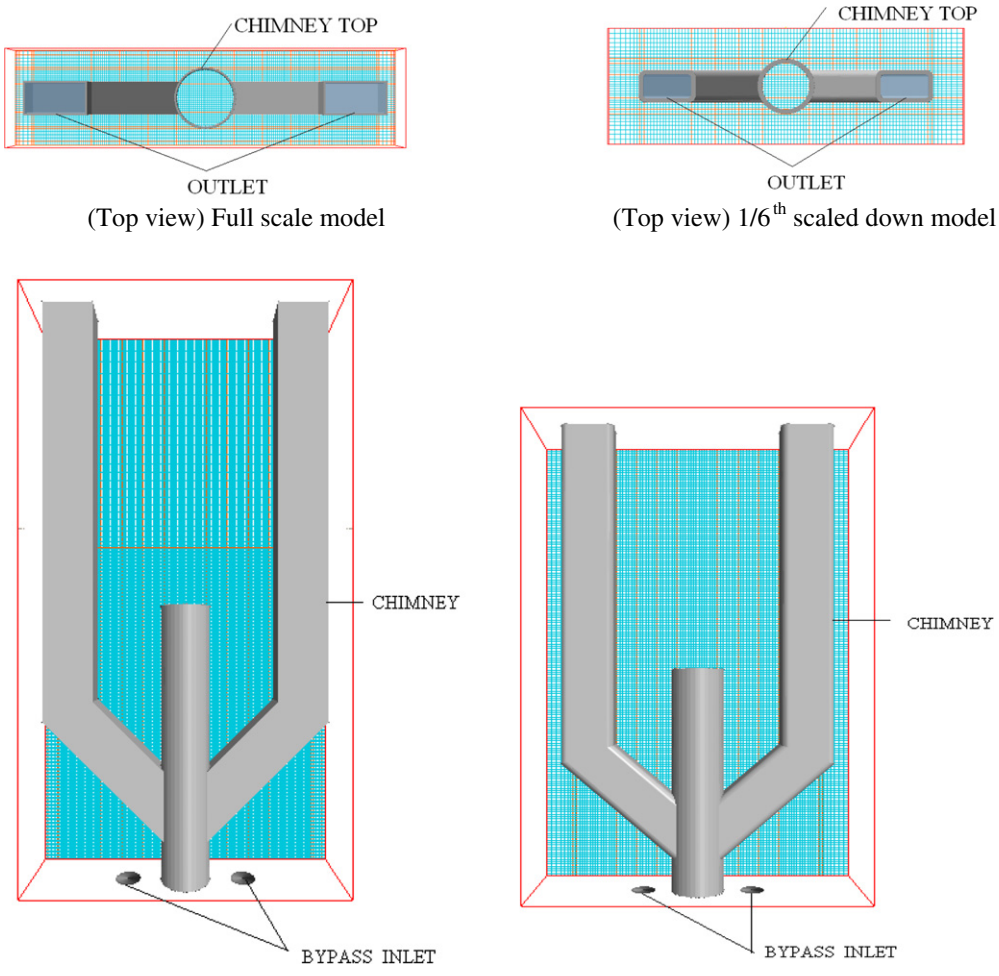

Fig. 3. Models prepared in PHOENICS for prototype and 1/6th scaled down model.

750 mm × 1250 mm × 250 mm. Calculation is done with (105 × 180 × 40) grid points. The models prepared in PHOENICS code for the prototype and 1/6th scaled down model are shown in Fig. 3.

5.2. Boundary conditions

The fluid domain material is considered as water and solid domain material as glass. The material properties are assumed to be constant. A uniform velocity profile has been set at the inlet. As a boundary condition, the inlet values of turbulent kinetic energy (k) and turbulence energy dissipation rate (ε) are prescribed in terms of the turbulence intensity (I). The k and ε is computed using the following relation.

$$k = (IU_{in})^2 \quad \text{and} \quad \varepsilon = 0.1643\frac{k^{3/2}}{l_m} \tag{7}$$

Here U_{in} is the bulk inlet velocity and l_m is the mixing length. As a general practice, mixing length is of the order of 10% of the characteristic inlet dimension (i.e., hydraulic radius for the inlet pipe). Turbulent intensity (I) is assumed to be 5%.

Considering chimney surface walls, no slip boundary condition is imposed on the surfaces. For the pool water domain boundary, zero gradient boundary condition is applied. Outlet boundary condition with fixed pressure is specified for the outlet nozzles on x–z plane (at y = 7.5 m for full scale and y = 1.25 m for the model). Inlet flow through the bottom of the chimney and bypass flow into the pool through the two bottom nozzles are specified based on the flow considered for the simulation case.

6. Validation

In order to ascertain the reliability of the CFD results obtained from PHOENICS, verification studies are tried with available numerical and experimental results. Though, provision of open chimney structure is being used by some research reactors (such as HANARO, ETRR-2, and OPAL) at the reactor core outlet to pre-

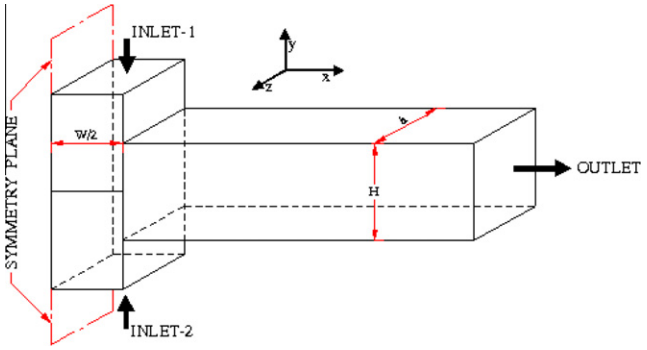

Fig. 4a. Half domain model for 3-D mixing of opposing jets (Wang and Mujumdar, 2005).

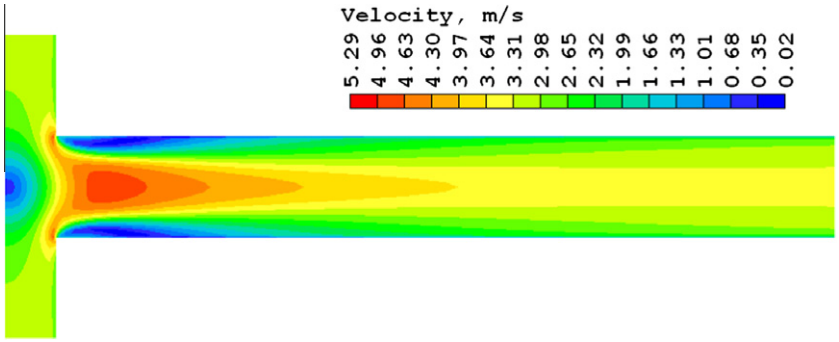

Fig. 4b. Velocity distribution for M = 1.

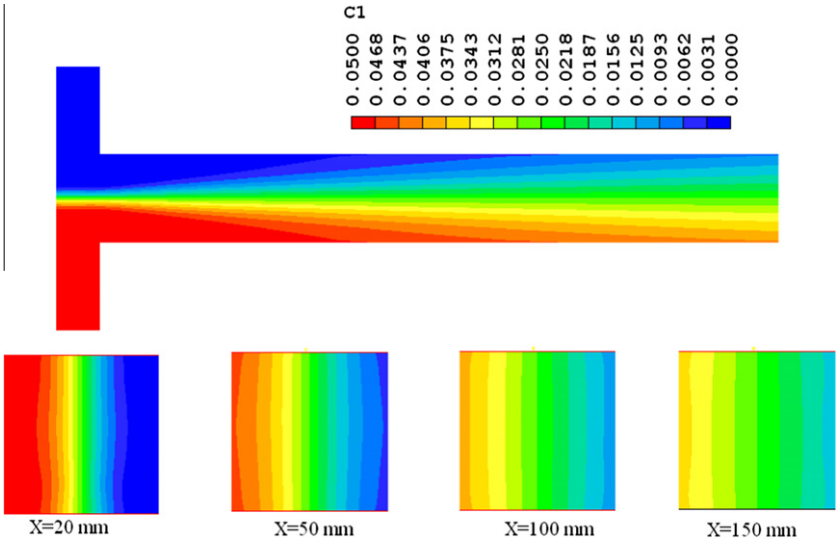

Fig. 4c. Concentration distribution for M = 1.

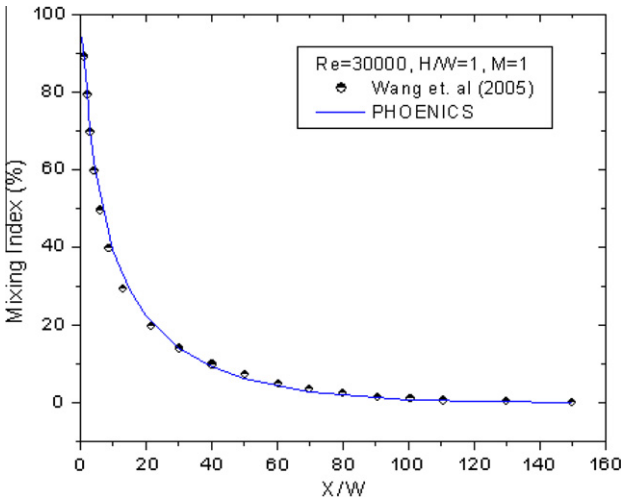

Fig. 4d. Variation of mixing index for $M = 1$.

vent mixing of radioactive coolant from the core with the bulk pool water, analysis of three dimensional studies have not been reported in literature to correlate parameters affecting the stagnation depth. A computational study considering steady, incompressible, irrotational flow for two-dimensional geometry has been reported by El-Morshdy (2007) for ETRR-2 reactor. Since the mixing flow of upward hot fluid and downward cold fluid just before the side nozzles of the chimney has similarity with respect to the impingement of opposing jets in a mixer, numerical results of Wang and Mujumdar (2005) have been taken for verification.

The three-dimensional numerical simulation of in-line static opposing jet mixer was reported by Wang and Mujumdar (2005) where pure water and sodium chloride solution were introduced at the nozzle inlets. After impingement in the mixer, the combined fluid leaves symmetrically via two symmetric exit channel outlets. Due to geometric and physical symmetry, only flow field within the half domain was solved numerically as shown in Fig. 4a. The boundary conditions were (i) uniform velocity, species concentration, turbulent kinetic energy and its dissipation rate at the nozzle inlets, (ii) symmetric boundary condition imposed along the symmetry plane, (iii) fully developed flow velocity considered at the outlet plane, and (iv) no-slip and insulated wall boundary conditions specified in the confinement walls.

For comparison purposes, three dimensional CFD simulation is carried out considering Re = 30,000 (based on the flow velocity and the hydraulic diameter of the outlet square cross section with $h/H = 1$) and $H/W = 1$ using PHOENICS code. The ratio of inlet mass flow rates of two jets considered in the simulation is 1. Concentration (C1) at inlet-1 is assumed to be 0.0 and that of inlet-2 is 0.05. The low Reynolds number k–ε turbulence models were used in this study. The velocity magnitude distribution results at centre plane (i.e. $z = 0$) are shown in Fig. 4b. The concentration distribution in the central plane ($z = 0$) is shown in Fig. 4c. In addition to this concentration distribution at four downstream locations ($x = 20$ mm, 50 mm, 100 mm and 150 mm) are also shown in this figure. These velocity distribution and concentration distribution show similar results as reported by Wang and Mujumdar (2005). Finally, mixing index (MI) as defined by Wang et al. is predicted using the following relations:

$$\mathrm{MI}(\%) = \frac{S_c}{C_b} \times 100 \tag{8}$$

$$S_c = \sqrt{\left[\sum_{i=1}^{n} (C_i - C_b)^2\right] \Big/ (n-1)} \tag{9}$$

$$C_b = \frac{\int Cu\, dA}{\int u\, dA} \tag{10}$$

The mixing index variation along the channel length (x-direction) is compared with the results reported by Wang et al. as shown in Fig. 4d. The results show good agreement between the results reported and results obtained by PHOENICS code.

A comparison is also made with the experimental data (with similar Reynolds number range based on pipe diameter) of Naik-Nimbalkar et al. (2010) using standard high Reynolds number standard k–ε turbulence model to understand the utility of PHEONICS code for mixing phenomena in T-junction. Table 4 shows the experimental condition for which the numerical simulation is carried out using PHOENICS code. The experiment of Naik-Nimbalkar et al. involved mixing of cold water and hot water in a T-junction test section as shown in Fig. 5a. T-junction was constructed of acrylic pipes. Cold water entered from horizontal main pipe and hot water entered from the branch pipe. Velocities and temperatures at the main and branch pipes were confirmed to be at steady-state

Table 4
Experimental condition for the cross flow experiment considered for simulation (Naik-Nimbalkar et al., 2010).

Parameters	Diameter (m)	Velocity (m/s)	Temperature (°C)	Reynolds number
Main pipe	0.05	1.0	30	Red $\sim 8 \times 10^4$
Branch pipe	0.025	0.5	45	Red* $\sim 2 \times 10^4$

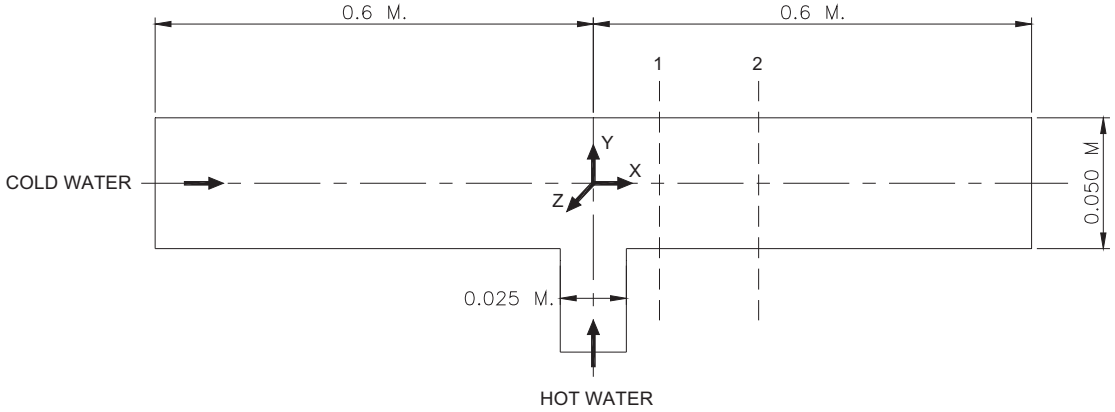

Fig. 5a. T-junction test section for cross flow experiment (Naik-Nimbalkar et al., 2010).

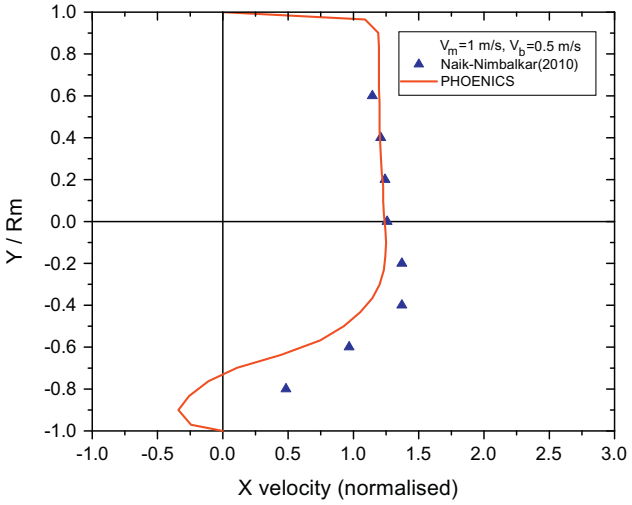

Fig. 5b. Normalised *x*-velocity at 0.5D downstream.

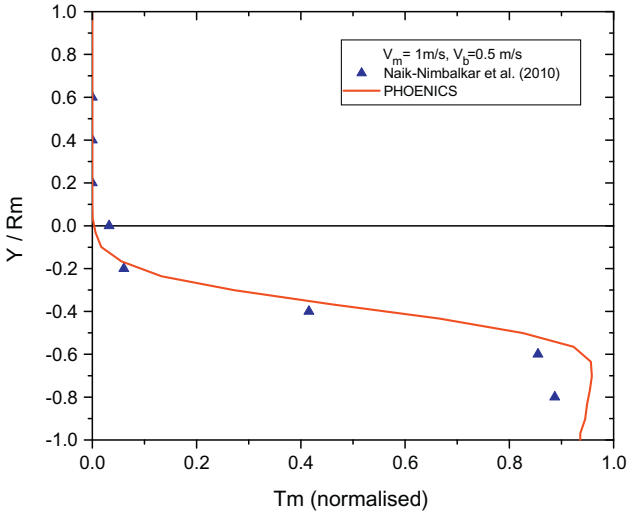

Fig. 5c. Normalised temperature at 0.5D downstream.

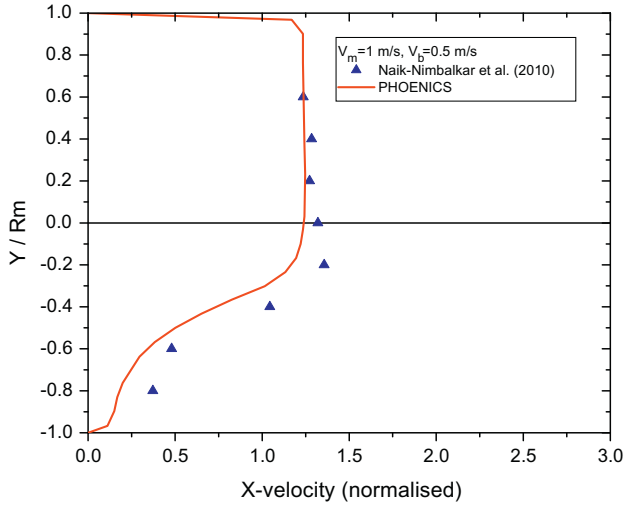

Fig. 5d. Normalised *x*-velocity at 1.25D downstream.

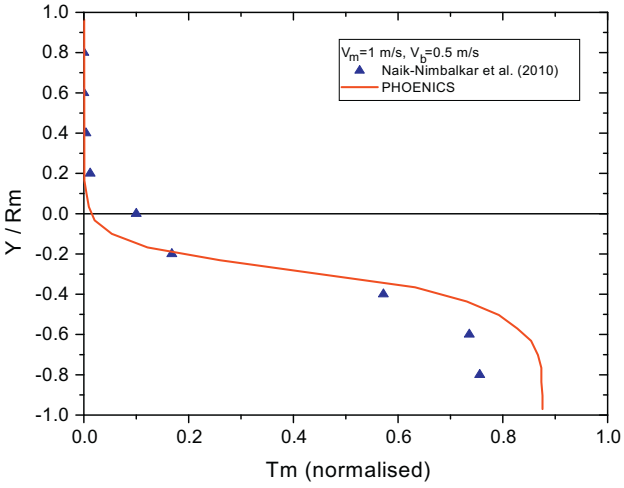

Fig. 5e. Normalised temperature at 1.25D downstream.

before each experiment was performed. Velocity and temperature measurements were carried out at two locations ((1) at 0.5D downstream and (2) at 1.25D downstream from $x = 0$) using hot-wire anemometer. A constant temperature module (CTA) was used for the measurement of local velocity in the system.

In the PHOENICS simulation the standard k–ε turbulence model is used. No slip and adiabatic boundary conditions are used for the wall. Boundary condition at inlet for this model is considered to be uniform velocity at 12D upstream condition. The outlet boundary condition is specified as constant pressure boundary condition. The variation in density of working fluid due to temperature change was considered using Boussinesq approximation. A comparison of the PHOENICS prediction with the experimental data is presented in Figs. 5b–5e. *x*-velocity is normalised with respect to the velocity of main pipe. The mean temperature of coolant is normalised using the following relation as defined by Naik-Nimbalkar et al. (2010), where T_h is hot water temperature and T_c is the cold water temperature.

$$\text{Normalised temperature} = \frac{T - T_c}{T_h - T_c} \tag{11}$$

The normalised *x*-velocity variation across *y*-direction in the central plan is compared at 0.5D downstream in Fig. 5b. The results for normalised *x*-velocity variation at 1.25D downstream are shown in Fig. 5d. Similarly normalised temperature variation across *y*-direction in the central plan is compared at 0.5D downstream in Fig. 5c and at 1.25D downstream in Fig. 5e. It is observed that the velocity as well as temperature distribution predicted by numerical simulation are in good agreement with the experiment.

7. Results and discussion

The results of the computational data matrix for the chimney scaled down model with the maximum flow (25 kg/s) and minimum flow (8.33 kg/s) considered for the experiment are discussed in details here. Velocity and temperature distribution for core flow of 25 kg/s is shown in Figs. 6–9. The velocity contour plots of the entire domain and the velocity vector plots in the central chimney region are shown in Fig. 6 for the two bounding cases i.e., bypass flow of 0% and 15%. When no bypass flow is provided (i.e., core bypass – 0%), net flow through the chimney top region is zero. The velocity contour plots of *x*–*y* plane and *y*–*z* plane for this case are shown in Fig. 6a(i) and a(ii) respectively. It is observed that from the bottom of the chimney, core flow enters at a velocity of about

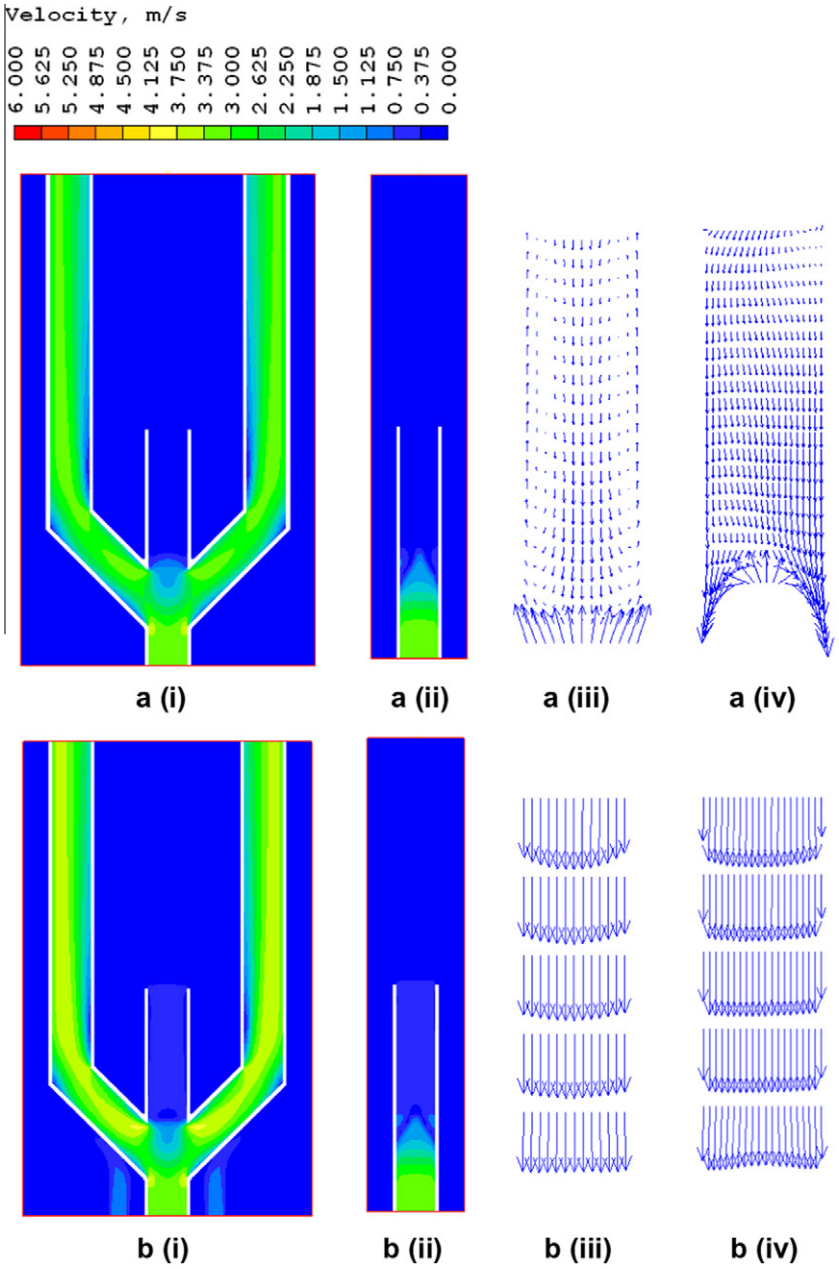

Fig. 6. Velocity distribution in model – core flow 25 kg/s, bypass (a) 0% and (b) 15%. (i) Contour plot in *x*–*y* plane, (ii) contour plot in y-z plane, (iii) vector plot in *x*–*y* plane, and (iv) vector plot in *y*–*z* plane.

3.2 m/s in the upward direction. This flow gets diverted through the two side rectangular opening of outlet nozzles. The velocity contours in the junction region of Fig. 6a(i) shows how main flow velocity (from the bottom entry of the chimney) gradually diminishes in the forward direction and gets distributed in the three adjacent openings. Velocity distribution in *y*–*z* plane shows the upward water jet in Fig. 6a(ii). Two vortices are seen by the two sides of the jet.

Since the side outlet nozzles are connected to the outlet (towards the pump suction) and top portion of the chimney is open to the pool, a downward velocity is observed in the chimney due to suction effect caused by pumping out of water through two outlet nozzles. Fig. 6a(iv) shows the velocity vectors for the top half of the chimney height (300 mm), which indicates the downward velocity profile. The bottom region of this vector plot shows the upward jet velocity effect of the core flow. Fig. 6a(iii) shows the vector plot in the *x*–*y* plane. Here it is observed that in the central region, flow velocity is downward. Since the net flow through the top portion of chimney is zero, flow balancing takes place through the peripheral region. This means a part of the core flow moves upward through this peripheral region and reaches to pool top. This is not acceptable because core outlet flow (which is radioactive) reaching the pool top leads to increase in pool top activity level. Therefore, these results clearly indicate that core bypass flow is necessary to avoid core outlet flow reaching the pool top.

When bypass flow is provided, there is a net downward flow through the chimney and therefore, core outlet water will not reach the pool top. Providing bypass flow eliminates the upward flow tendency in the peripheral region and complete downward velocity field in the top chimney region is observed for various cases of flow bypass (5%, 10% and 15%). As a bounding case, results of 15% are discussed below.

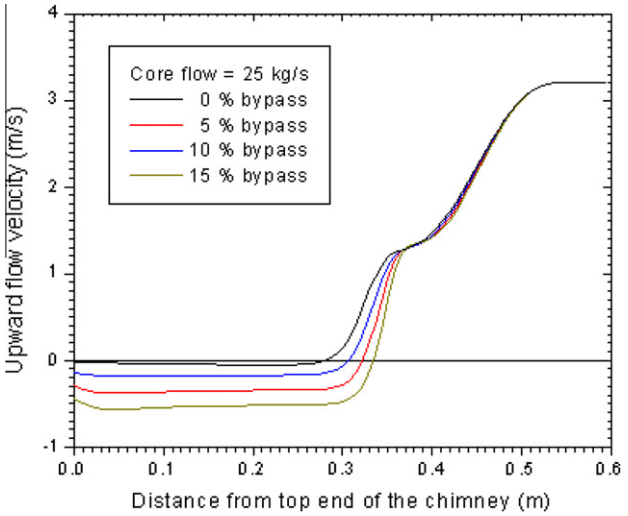

Fig. 7. Centre line velocity variation along the height of chimney model (core flow 25 kg/s).

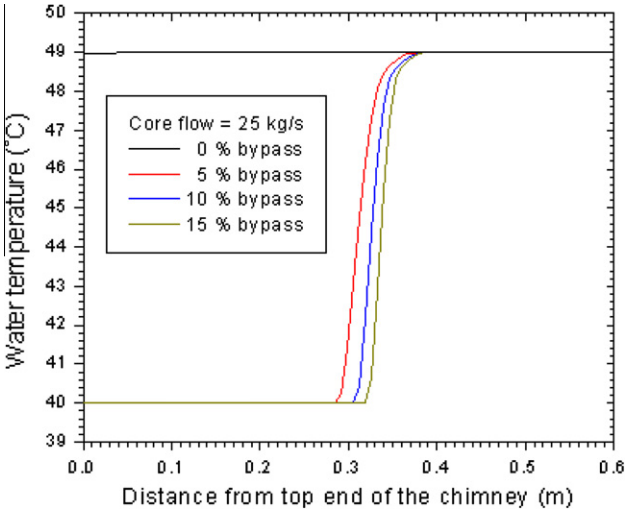

Fig. 9. Centre line water temperature variation along the height of chimney model (core flow 25 kg/s).

For 15% core bypass flow, the velocity distribution in x–y plane and y–z plane is shown in Fig. 6b(i) and b(ii) respectively. From the bottom plane of the pool, 7½% of the core flow is sent through each bypass path as shown in Fig. 6b(i). The bypass flow enters at a velocity of about 0.95 m/s into the pool through each path. This water finally enters through the top end of the chimney and moves with a velocity of about 0.5 m/s. Fig. 6b(ii) shows that the velocity distribution in the y–z plane. The upward flow jet in the central region is observed along with recirculation regions in this figure. The extent of upward jet of core flow is observed to be less with respect to Fig. 6a(ii). This is because the downward flow velocity (0.5 m/s) suppresses the upward jet velocity (3.2 m/s) from the core outlet. The extent of two vortices by the sides of the upward jet in the vertical direction is also smaller than that observed in Fig. 6a(ii).

Fig. 6b(iii) and b(iv) shows the velocity vector plots in the x–y plane and y–z plane respectively, which indicate the downward velocity profile through the top half of the chimney. The velocity vector plots in y–z plane shows that the height of the upward jet canopy decreases with provision of bypass flow.

To understand the extent of suppression of the upward jet for various bypass flow cases (0%, 5%, 10% and 15%), upward velocity variation are plotted along the height of the chimney in the central plane of the chimney as shown in Fig. 7. It is observed that the upward flow velocity in the central axis of the chimney reduces from 3.2 m/s to zero and finally becomes negative (i.e., flow is downward) towards the upper part of the chimney. The location of zero velocity indicates the location where upward water jet motion stops. As core bypass flow increases, this location (of zero velocity) shifts away from the top end of the chimney. The distance from the top end of the chimney to this location is called stagnation depth. In case of 0% core bypass flow, the central upward jet velocity is found to be zero at about 283 mm from the top end of the chimney (i.e., stagnation depth is 283 mm). Form the figure, it is clear that the stagnation depth increases with increase in bypass flow. When bypass flow changes, the stagnation depth varies because the ratio of the mass flow rate of the two opposing jets (hot upward core flow and cold downward bypass flow) changes. Core flow remaining constant, increase in bypass flow reduces the mass flow ratio

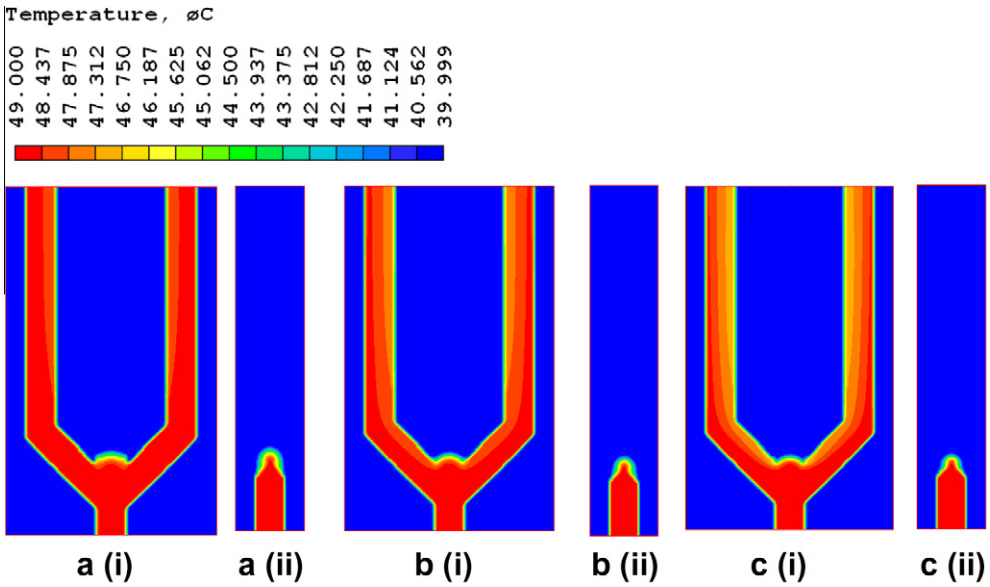

Fig. 8. Temperature contours – core flow 25 kg/s, bypass (a) 5%, (b) 10% and (c) 15%. (i) Contour plot in x–y plane and (ii) contour plot in y–z plane.

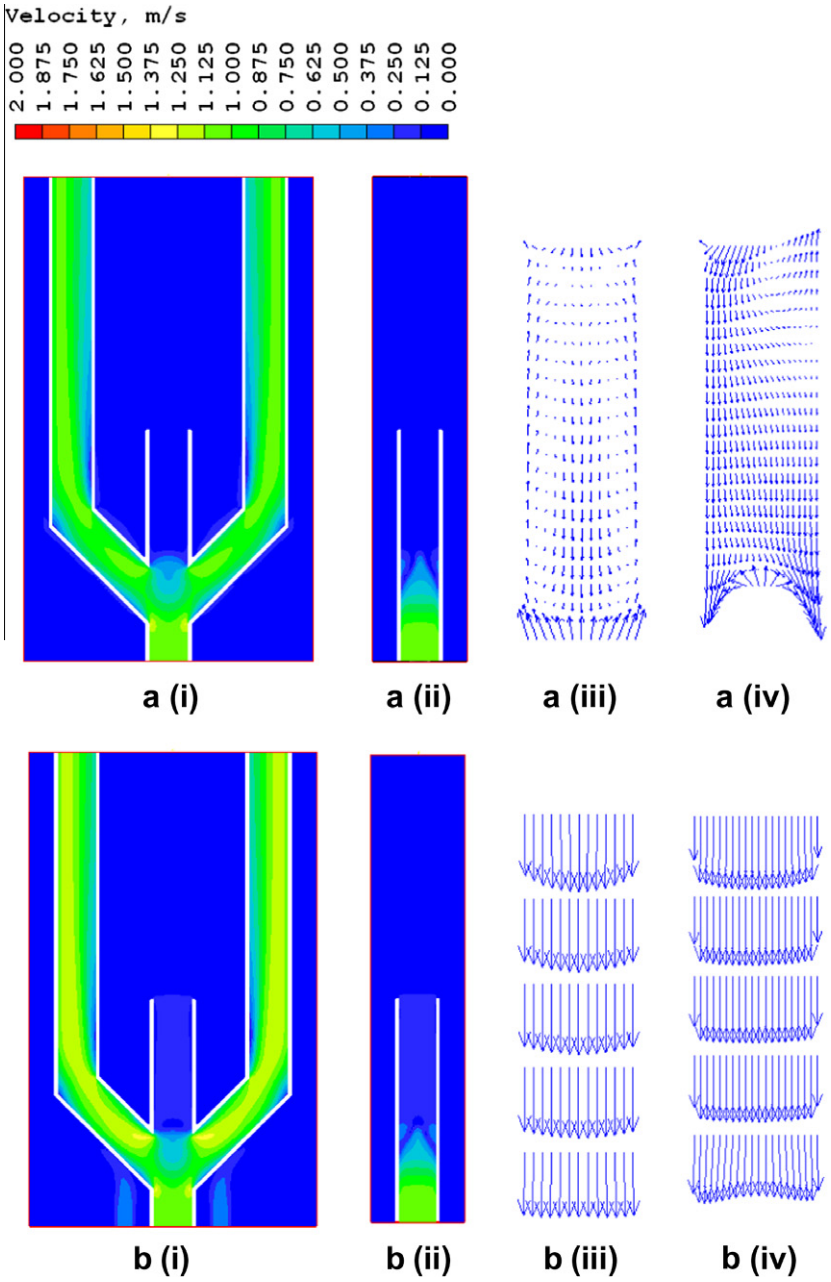

Fig. 10. Velocity distribution in model – core flow 8.33 kg/s, bypass (a) 0% and (b) 15%. (i) Contour plot in *x*–*y* plane, (ii) contour plot in *y*–*z* plane, (iii) vector plot in *x*–*y* plane, and (iv) vector plot in *y*–*z* plane.

M_R. Here M_R is defined as the ratio of mass flow rate through the core (i.e., core flow) to the mass flow rate passing through the top of the chimney (i.e., bypass flow). Since the mass flow rates are not equal, inlet momentum of both the jets are different. The opposing jets impinge head-on a plane towards the weaker jet before being sucked out through the side outlet nozzles. With increase in bypass flow (downward) from the top of the chimney, inlet downward momentum increases with respect to the upward momentum of the core flow. Thereby, the plane at which head-on impingement takes place, shifts downward and the distance from the top edge of the chimney to the plane of impingement (which is expressed as stagnation depth) increases. With 15% bypass flow, the stagnation depth is observed to be 335 mm, which means that suppression of upward jet takes place by a distance of 52 mm (i.e., 335–283 mm) due to this additional flow of 15% core bypass.

The temperature distribution due to mixing of hot fluid and cold fluid inside the chimney model considering core flow of 25 kg/s is also analysed. The upward flowing hot water jet is at 49 °C and bypass flow water temperature is 40 °C. It is observed that pool water temperature stabilises at 49 °C (i.e. core outlet temperature) if no core bypass flow is sent into the pool. Water temperature establishes at the core outlet temperature because hot water form the core outlet reaches the chimney top opening through the peripheral region as described earlier. When bypass flow is provided, pool water is sucked inside the chimney. However, due to upward flowing hot fluid from the bottom of the chimney, pool water front (40 °C) reaches only up to a certain depth with respect to the top end of the chimney. Fig. 8a(i), b(i) and c(i) shows the temperature contour plots in *x*–*y* plane for 5%, 10% and 15% core bypass flow cases respectively. Temperature at the outlet nozzles gradually de-

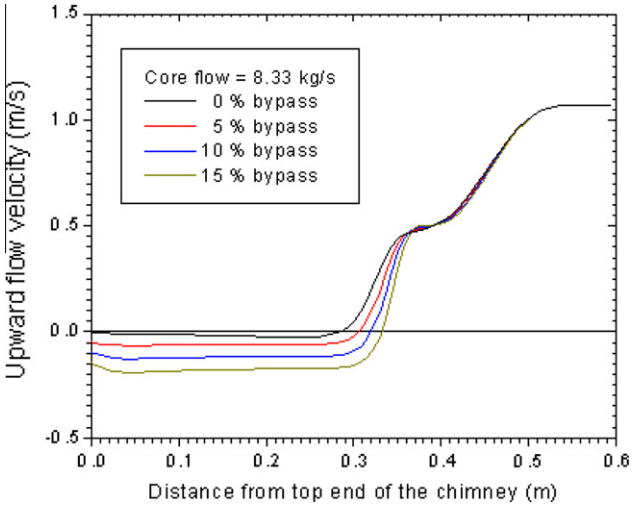

Fig. 11. Centre line velocity variation along the height of chimney model (core flow 8.33 kg/s).

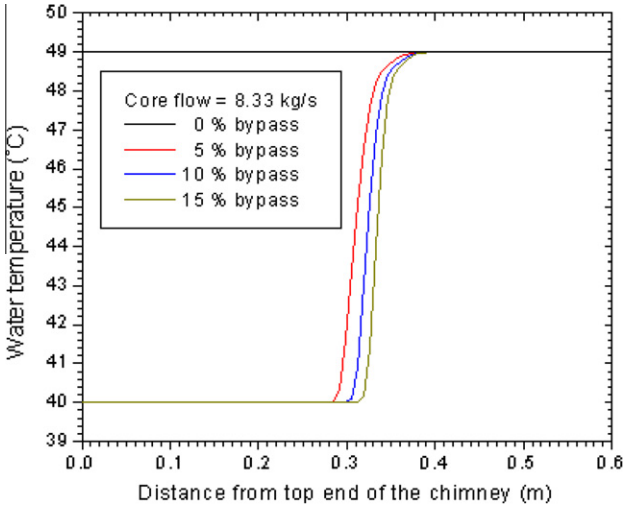

Fig. 13. Centre line water temperature variation along the height of chimney model (core flow 8.33 kg/s).

creases with increase in bypass flow. A temperature gradient exists from inner face of the vertical outlet channel (i.e. nearer to the vertical central axis of chimney) to the outer face of the channel. It is found that inner face temperature is lower than that of the outer face. This is because the pool water, which is at a lower temperature, gets a preferential path to be sucked in adjacent to the inner face of the outlet channel.

Fig. 8a(ii), b(ii), and c(ii) shows the temperature contour plots in y–z plane for 5%, 10% and 15% core bypass flow cases respectively. Here, the core outlet temperature (49 °C) is thought to be a tracer of radioactive water and pool temperature (40 °C) is non-radioactive water. When bypass flow is sent into the pool, this pool water temperature front reaches inside the chimney. Therefore, non-radioactive region of the chimney is equivalent to the depth up to which pool temperature front reaches inside the chimney. A new parameter – pool water temperature front depth is defined as the distance from the top edge of the central chimney to the location up to which chimney centre line temperature is equal to 40 °C.

Pool water temperature front depth variation for various bypass flow is evaluated from Fig. 9. Here the water temperature in the central axis of chimney is plotted along the height of the chimney. For 0% core bypass, water temperature is 49 °C throughout the chimney, This signifies that radioactivity will spread throughout the pool in case no bypass flow is provided into the pool (as explained earlier that pool water temperature establishes to 49 °C). For 5% core bypass, water temperature is 40 °C up to a distance of 286 mm from the top end of the chimney (i.e., pool water temperature front depth is 286 mm). With increase in bypass flow to 10% and 15%, this temperature front depth increases to 305 mm and 319 mm respectively.

The results of the case with minimum core flow (i.e., 8.33 kg/s) for the scaled down model are shown in Figs. 10–13. This is the case, which is able to satisfy the Richardson number expected for the prototype as indicated in Table 2b, so that relative effect of buoyancy force with respect to the inertia force is established through the simulation. Though magnitude of flow velocity is about 1/3rd of the previous case, similar results is observed as described earlier considering similar core bypass percentage. The velocity contour plots for 0% core bypass in x–y plane and y–z plane are shown in Fig. 10a(i) and (ii) respectively. Similar diversion of flow and mixing is observed in x–y plane. Core outlet flow moves

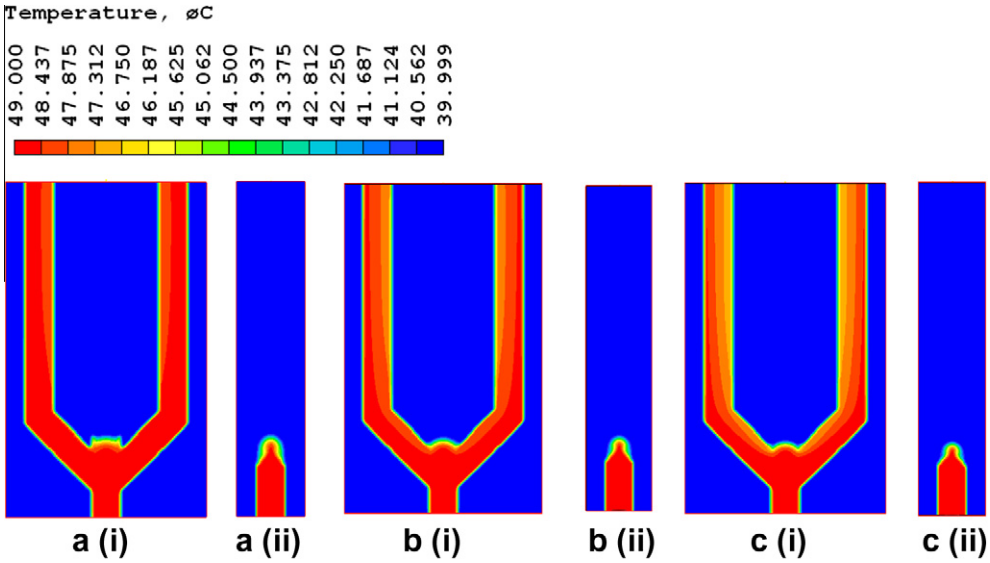

Fig. 12. Temperature contours – core flow 8.33 kg/s, bypass (a) 5%, (b) 10% and (c) 15%. (i) Contour plot in x–y plane and (ii) contour plot in y–z plane.

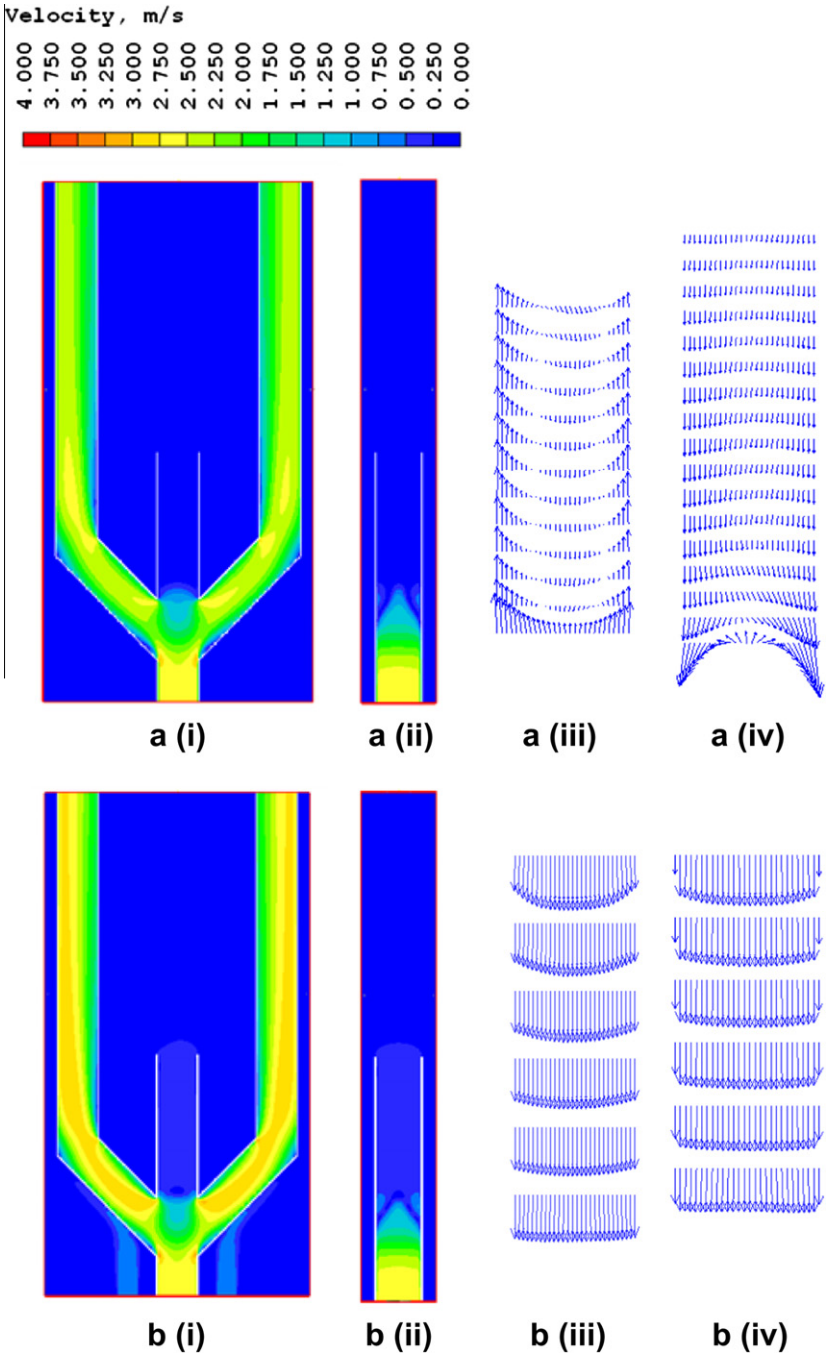

Fig. 14. Velocity distribution in prototype – core flow 750 kg/s, bypass (a) 0% and (b) 15%. (i) Contour plot in *x*–*y* plane, (ii) contour plot in *y*–*z* plane, (iii) vector plot in *x*–*y* plane, and (iv) vector plot in *y*–*z* plane.

upward with a velocity of about 1.05 m/s through the bottom end of the chimney. During diversion, similar water jet behaviour along with recirculation zone is observed in the *y*–*z* plane. Fig. 10a(iii) and a(iv) shows the velocity vector plots in *x*–*y* plane and *y*–*z* plane respectively. It is observed in Fig. 10a(iii) that the flow direction is downward in the central region of the chimney and upward flow takes place through the peripheral region as observed in Fig. 6a(iii). Complete downward flow is observed in Fig. 10a(iv) and at the bottom portion, the canopy height of the jet and recirculation region is observed to be lower than that of Fig. 6a(iv).

Fig. 10b(i) and b(ii) shows the velocity distribution in *x*–*y* plane and *y*–*z* plane respectively for 15% core bypass flow case. The velocity vector plots in *x*–*y* plane and *y*–*z* plane are shown in Fig. 10b(iii) and b(iv) respectively. These results are similar to that observed in Fig. 6b(i)–b(iv).

Variation of upward velocity (i.e., *y*-component) at the central axis of the chimney along the height is plotted for various bypass flow cases (0%, 5%, 10% and 15%) as shown in Fig. 11. These results show how stagnation depth varies for bypass flow cases. Stagnation depth for 0% bypass is observed to be 286 mm as against stagnation depth of 283 mm for 25 kg/s flow case in Fig. 7. The increase in stagnation depth from 283 mm to 286 mm is due to the lower velocity of the upward jet for this case with that of the previous case. Stagnation depth for 15% bypass case is observed to be about 332 mm as against 335 mm for the case with 25 kg/s core flow. The decrease in stagnation depth is due to lower (1/3rd) downward

velocity of the bypass flow. However it is observed that this variation in stagnation depth due to change in core flow from 25 kg/s to 8.33 kg/s has marginal effect. Whereas, for a specific core flow, variation of percentage bypass flow has a larger effect on the stagnation depth.

The results of temperature variation for the minimum core flow of 8.33 kg/s are shown in Fig. 12 (for 5%, 10% and 15% bypass flow cases). The temperature distribution is observed to be similar to that of core flow of 25 kg/s. The results show that with increase in bypass flow, the temperature front of the pool water (i.e., 40 °C) reaches deeper inside the chimney. The depth at which pool water front reaches are clearly seen in Fig. 13. As described earlier, for 0% bypass flow, the pool water temperature stabilises at 49 °C. When bypass flow is provided pool water temperature is maintained at 40 °C. For 5% bypass flow, pool water temperature front (i.e. 40 °C) is observed up to a depth of 285 mm from the top. For 10% and 15% bypass flow, this depth is about 300 mm and 312 mm respectively.

Numerical simulation results for the full scale prototype with 750 kg/s core flow is shown in Fig. 14. The flow velocity in the upward direction is about 2.6 m/s at the bottom entry location of the chimney. For 0% bypass flow case, the velocity contours in x–y plane and y–z plane are shown Fig. 14a(i) and a(ii) respectively. Similar jet behaviour in the y–z plane along with recirculation zone is observed in the prototype also. The velocity vectors in x–y plane and y–z plane are shown in Fig. 14a(iii) and a(iv) respectively. In prototype also, the velocity direction in the peripheral region is also observed to be upward in the x–y plane. For 15% core bypass flow, the velocity vectors in the x–y plane and y–z plane are shown in Fig. 14b(i) and b(ii). It is observed that the extent of jet size in the vertical direction is reduced. Velocity vector plots are shown in Fig. 14b(iii) and b(iv). The velocity distribution pattern inside the chimney for the prototype is found to be similar to that of the model. When comparison is made to see the effect of core bypass flow on stagnation depth for the prototype (Sengupta et al., 2011a,b), similar behaviour as indicated on the model are observed. For 5%, 10% and 15% bypass flow, the temperature front of pool water is found at depth of 1.68 m, 1.78 m and 1.84 m respectively from the top end of the chimney.

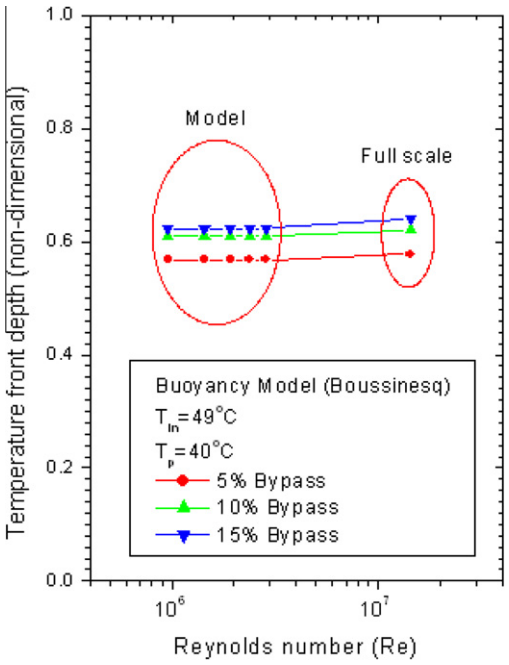

Fig. 16. Variation of temperature front depth (non-dimensional) with Reynolds number (Re).

To compare the results of prototype and model, non-dimensional stagnation depth variation is plotted with Reynolds number (Re) in Fig. 15. It is observed that almost a linear relationship exists between the prototype and the model. The results show that the velocity ratio between the core flow and core bypass is the major governing criteria to decide the stagnation depth. The results show that the non-dimensional stagnation depth increases with increase in Reynolds number for a specified percentage bypass flow (i.e., 5%, 10% or 15%). However, with no bypass flow (i.e., 0% bypass), non-dimensional stagnation depth decreases with increase in Reynolds

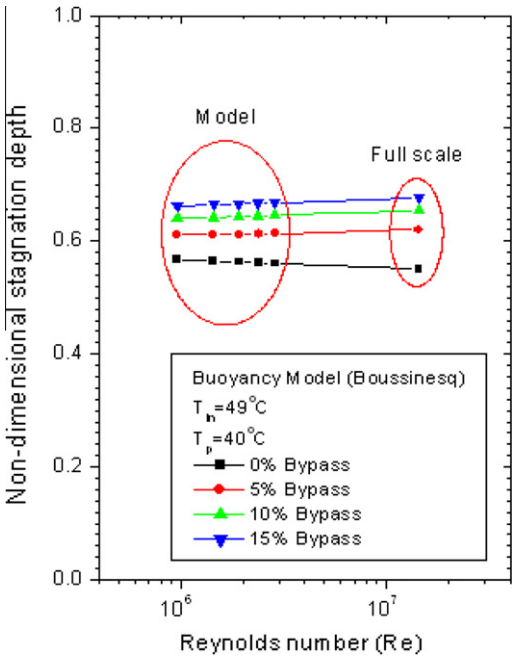

Fig. 15. Variation of non-dimensional stagnation depth with Reynolds umber (Re).

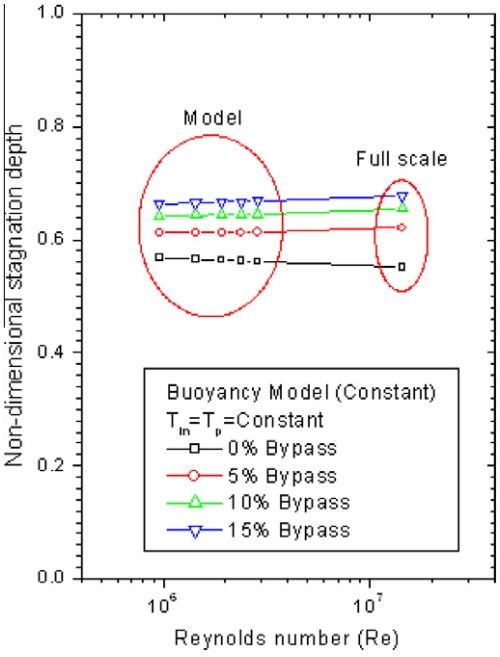

Fig. 17. Variation of non-dimensional stagnation depth with Reynolds number (Re) with $\Delta T = 0$ °C.

number. This is because in absence of bypass flow, as core flow velocity increases (i.e., increase in Reynolds number), the upward jet reaches to a larger height (i.e., towards the top end of the chimney). Thereby, stagnation depth decreases. On the contrary, when bypass flow is provided from the top, the impingement momentum between the two opposing jets increases with increase in Reynolds number. This reduces the height of the jet and recirculation zone causing stagnation depth to increase.

The pool water temperature front depth is normalised with chimney height (L) to define the parameter called non-dimensional pool water temperature front depth. The variation of non-dimensional temperature front depth with respect to the Reynolds number is shown in Fig. 16 for various cases of the scaled down model and the prototype. The results show similar relationship of the prototype and the model for 5%, 10% and 15% bypass flow cases. However, it is observed for the prototype that the pool water temperature front reaches deeper than that of the model leading to a lager non-dimensional temperature front depth.

To understand the effect of temperature difference on location of stagnation point, computations were done considering hypothetically core outlet water and pool water temperature as equal. The results are shown in the form of non-dimensional stagnation depth variation with the Reynolds number as shown in Fig. 17. These results show that the effect of temperature difference between the core outlet and pool water on the stagnation depth is marginal.

8. Conclusions

The turbulent mixing behaviour of upward flowing hot fluid and downward flowing cold fluid inside the chimney of the 1/6th scaled down model and that of the prototype for a pool type research reactor is described. The effect of core bypass flow on stagnation depth is computed. Non-dimensional stagnation depth variation with respect to the Reynolds number for the model and the prototype shows similar relationship. It is observed that with increase in bypass flow, rate of rise of non-dimensional stagnation depth decreases. The effect of temperature difference on stagnation depth is found to be marginal. The ratio of core bypass flow and the core flow is the major parameter which decides the stagnation depth. It is observed that provision of core bypass is a necessity to maintain downward flow in the chimney and thereby achieving the objective of preventing the radioactivity reaching to the pool top.

References

Chafle, S.B., Sengupta, S., Mukherjee, P., Sasidharan, K., Raina, V.K., 2009. High Flux Research Reactor, Peacefulatom 2009, Thematic Volume – Reactor Systems and Applications, pp. 195–200.

El-Morshdy, S.El.-Din., 2007. Analytical study of the closure flow inside the ETRR-2 core chimney. Ann. Nucl. Energy 34, 228–232.

Ludwig, J.C., 2004. Concentration, Heat and Momentum Limited (CHAM). POLIS: Phoenics On-line Information System, London.

Naik-Nimbalkar, V.S., Patwardhan, A.W., Banerjee, I., Padmakumar, G., Vaidyanathan, G., 2010. Thermal mixing in T-junctions. Chem. Eng. Sci. 65, 5901–5911.

Patankar, S.V., 1980. Numerical Heat Transfer and Fluid Flow. Hemisphere Publication.

Sengupta, S., Singh T., Vijayan, P.K., Sasidharan, K., Raina, V.K., 2010a. Subchannel analysis of a high flux research reactor. In: 20th National and 9th International ISHMT-ASME Heat and Mass Transfer Conference, pp. 821–829. doi: 10.3850/9789810838133_221. ISBN: 978-981-08-3813-3.

Sengupta, S., Vijayan, P.K., Chafle, S.B., Sasidharan, K., 2010b. Design of a scaled test facility to simulate turbulent mixing inside the chimney of a pool type research reactor. In: 37th National and 4th International Conference on Fluid Mechanics and Fluid Power, FMFP10-NE-02. ISBN: 978-81-910571-1-9.

Sengupta, S., Vijayan, P.K., Sasidharan, K., Raina, V.K., 2011a. Turbulent mixing inside the chimney model of a pool type research reactor. In: 19th International Conference on Nuclear Engineering, Japan. ICONE19-43613.

Sengupta, S., Vijayan, P.K., Sasidharan, K., Raina, V.K., 2011b. Turbulent mixing of hot upward flow and cold downward flow inside the chimney of a pool type research reactor. In: 21st International Conference in Reactor Technology (SMiRT 21), Div-III: Paper ID-458.

Wang, S.J., Mujumdar, A.S., 2005. A numerical study of flow and mixing characteristics of three dimensional confined turbulent opposing jets: unequal jets. Chem. Eng. Process. 44, 1068–1074.